

A CASE STUDY ON 3-D RECONSTRUCTION AND SHAPE DESCRIPTION OF PEROXISOMES IN YEAST

J. Selinummi^{1*}, *A. Niemistö*^{2,1}, *R. Saleem*², *G.W. Carter*², *J. Aitchison*²,
*O. Yli-Harja*¹, *I. Shmulevich*², and *J. Boyle*²

¹Institute of Signal Processing, Tampere University of Technology,
P.O.Box 553, FI-33101 Tampere, Finland

²Institute for Systems Biology,
1441 North 34th Street, Seattle, WA 98103, USA
jyrki.selinummi@tut.fi

ABSTRACT

Subcellular organelles are commonly analyzed using 2-D fluorescent microscopy. However, 3-D reconstruction and analysis of organelle topology in a high-throughput manner promises to result in a better understanding of cellular systems. We developed image analysis methods for automated quantitative analysis of peroxisome shapes. The methods employ 3-D image stacks obtained by confocal microscopy. There are three fundamental phases: image preprocessing and segmentation, 3-D reconstruction, and automated quantification of peroxisome topology in 3-D using shape descriptors. The algorithms are shown to produce results that can be used to classify objects of different topologies, and to enable visual studies of peroxisomes in 3-D.

Index Terms— Biological cells, image analysis, image reconstruction, biomedical image processing

1. INTRODUCTION

3-D imaging, reconstruction, and automated analysis are common tools in several disciplines. In magnetic resonance and PET imaging, 3-D reconstruction is used in producing the final output image that is then analyzed visually, or using automated analysis [1]. 3-D techniques are also used in, for example, describing the shape and deformation of heart during a beat [2]. In computer graphics and in computer aided design, browsing through databases containing 3-D models often requires automation of shape description and 3-D shape matching [3]. In material sciences, 3-D imaging and shape description can be used in, for example, studying mechanical properties of concrete [4].

In this paper, we study 3-D reconstruction and shape description in the context of peroxisomes in yeast. Peroxisomal defects underlie a large number of human health concerns, including diabetes, cancer, and heart disease. In yeast, peroxisomes are inducible, independent subcellular organelles, whose development involves a limited number of genes with numerous human counterparts, making peroxisomes an ideal model system to apply a systems biology approach. Previously, we have used 2-D imaging to extract the number of peroxisomes in yeast [5], but in order to enable more detailed shape description, 3-D analysis is needed.

In the field of cytometry, although confocal microscopy inherently enables 3-D imaging, often only a 2-D projection is used

in the actual study of the specimen. 2-D representation saves storage space and prevents visualization problems of 3-D reconstruction: it is faster and more convenient to project the data into a 2-D image with mean or maximum projections. Furthermore, it is not trivial to produce an illustrative view of several 2-D slices in the z dimension and finally perform 3-D digital image analysis in a fully automated manner. While there has been interest in 3-D reconstruction of subcellular structures from microscopy images, the work has most often been performed using electron microscopy [6, 7], or the context has not been high-throughput experiments [8].

We present an automated, straightforward, and high-throughput approach for the visualization and shape description of yeast peroxisomes in 3-D. Using a confocal microscope, we show that it is beneficial to store and use all the z -slices produced by the microscope, and not just the 2-D projections. In comparison to 2-D digital image analysis, our approach can be used, for example, to increase the accuracy of peroxisome enumeration in high-throughput applications, or to describe peroxisome shapes under different conditions. The presented methods are fully automated, which is to say that no user intervention is needed.

2. MATERIALS AND METHODS

In order to enable a high-throughput study of the shapes of peroxisomes in yeast, we need to incubate the cells, image the populations, store the images, and analyze the images using digital image analysis.

2.1. Cell Incubation and Imaging

We utilized a green fluorescent protein (GFP) based reporter assay as our primary tool to investigate peroxisome induction. The gene encoding the yeast peroxisomal matrix enzyme, 3-ketoacyl-CoA thiolase (POT1), was C-terminally tagged with the GFP gene by homologous recombination creating a genomically integrated copy of POT1GFP in the *Saccharomyces cerevisiae* strain BY4742.

Cells were grown to log phase in glucose-containing media, then shifted to oleate containing media and induced for 6 hours, inducing peroxisome biogenesis and concomitant POT1GFP expression. Cells were fixed at the given time point in 3.7% formaldehyde and washed in phosphate buffered saline solution. Confocal images were taken as a series of 20 slices through the z axis, utilizing line averaging to suppress noise.

*The first author performed the work while at the Institute for Systems Biology, Seattle, WA, USA

2.2. Automated Image Analysis

The fluorescent image stacks of peroxisomes were automatically stored in a file server using a standardized naming convention to enable easy automation of the digital image analysis. The analysis is divided into three phases, each designed for high-throughput measurements through low computational cost.

2.2.1. Preprocessing

The 3-D input image consists of several 2-D images taken with different focus levels in the z dimension. For each of the z -slices, we first perform standard 2-D median filtering in a 3×3 window to remove impulse noise present in the confocal images. The filtered image is then thresholded using a threshold obtained by Otsu's method [9]. Since we expect that peroxisomes are visible as bright spots over a dark background, with approximately 1% – 5% of all the pixels in the image representing the peroxisomes, we can discard thresholding results that are likely to be erroneous. Specifically, we discard a z -slice if the thresholding indicates that over 10% of the pixels are foreground pixels. This approach works in practice because if the image consists of only noise, it is very likely that a significant portion of the image is thresholded as foreground (and therefore discarded), while if peroxisomes are present the foreground only consists of approximately 1% of pixels as mentioned above.

After the binarization by thresholding of each image, we stack the images which were not discarded to form a 3-D binary matrix, where 1's indicate peroxisome pixels and 0's the background. For example, if we have 512×512 images for each z position, and use 20 different z depths, we get a $512 \times 512 \times 20$ matrix of 1's and 0's. Next, we remove objects that are significantly too small or too large to be peroxisomes. The size thresholds were determined manually by an expert, and were consistently used in all tests presented in this paper.

The resolution of confocal microscopes is often anisotropic. In our study, the resolution of the z dimension is not as high as the resolution in x and y directions, and we therefore interpolate new z values to the 3-D stack by nearest neighbor interpolation. New values are also interpolated to compensate for the images discarded because of erroneous thresholding. All further processing, visualization, and measurement steps are performed to the interpolated stack. Since the aim is to enumerate the peroxisomes and describe the shapes peroxisome-by-peroxisome, we apply the 3-D watershed transform with h-minima suppression to separate possibly overlapping objects [10].

2.2.2. 3-D reconstruction

After preprocessing, we have a 3-D binary matrix with peroxisomes and background, where each peroxisome is separated with at least one or more background pixels. Since the pixels now have x , y and z coordinates, we refer to them as voxels, the 3-D equivalent of a pixel. Similarly to how pixels describe the intensity of a small area in an image, each voxel describes the intensity of a small volume in 3-D space.

There are two main approaches to 3-D reconstruction, the volumetric reconstruction and surface reconstruction. The volumetric reconstruction follows naturally from the coordinates of the voxels in 3-D space: since one voxel defines the intensity of a small volume in 3-D, we draw a semi-transparent $1 \times 1 \times 1$ cube in the location of each 1 in the matrix. In surface reconstruction the aim is to locate the surface of the object, model it using faces and vertices, and apply some lighting method [11] to visualize the surface. The modeling of the surface is a nontrivial task, and is an active area of research. There are several algorithms in the literature: we used the built-in MATLAB (The MathWorks, Inc., Natick, MA) function "isosurface".

2.2.3. Shape analysis

Although we know the coordinates of the voxels that comprise the peroxisomes, we still need methods to efficiently classify different peroxisomes by their shape and intensity. In 2-D image analysis, shape descriptors [12] are used extensively, for example, to describe the shapes of intracellular structures [13]. Many of the descriptors can be extended into 3-D in a straightforward manner. First, we perform normalization by translating the center of mass of the peroxisome to the origin. Second, using principal component analysis on the covariance matrix of the coordinates of the voxels, we rotate the peroxisome by aligning the coordinate axes to the directions of the eigenvectors corresponding to the largest eigenvalues. This procedure aligns the peroxisome along the coordinate axis and provides adequate rotation invariance.

After the normalization we measure the following descriptors for each peroxisome:

Volume The number of voxels in the peroxisome.

Length, width and thickness The maximum distances between two voxels in the direction of the three eigenvectors corresponding to the three largest eigenvalues, respectively.

Orientation The direction of the eigenvector corresponding to the largest eigenvalue.

Median intensity The median of intensities of the peroxisome voxels, measured from the original stacked z -slices.

Compactness Measure of the roundness of the object shape. Classical compactness defined as $(\text{Area}^3/\text{Volume}^2)$, minimized by a sphere.

Convexity Measure of complexity of the object. Defined as the volume of the object divided by the volume of the convex hull of the object, maximized by a convex object.

3. CASE STUDY

The analysis procedures described in the previous section were tested on an image set consisting of 20 confocal stacks, each of which were 512×512 pixels in size.

Figure 1 shows the preprocessing phases, forming the z -slices of GFP stained peroxisomes into a binary 3-D matrix. In Figure 2, the differences between two 3-D reconstruction techniques are presented. The volumetric reconstruction emphasizes the locations of the individual voxels, and is therefore very useful in a detailed study of the shape of the peroxisome and the quality of the segmentation, when zooming on the object. Using this approach, however, the overall shape and 3-D depth of the object is hard to visualize. The surface reconstruction, on the other hand, gives visually very appealing reconstruction, interpolating a smooth surface and including lighting. While for visualization purposes the latter method is more attractive, we suggest that the actual measurements and visual study of the details be done using the volumetric method if the visualization software gives the possibility to rotate and zoom in.

In Figure 3, the separation of overlapping objects in 3-D is presented. Figure 3 (A) shows the 2-D projection of the peroxisome data. Although the peroxisome is somewhat narrower in the center, it would still be difficult to decide whether there are one or two peroxisomes in the cluster. In Figure 3 (B), however, the rotated 3-D representation makes the narrowing much clearer, and the watershed segmentation succeeds in the separation as seen in Figure 3 (C).

As a proof of principle to illustrate the usefulness of the selected shape descriptors, we calculated the descriptors first for the peroxisome complex in Figure 3 (B), and then for both of the separated peroxisomes in Figure 3 (C). These objects were

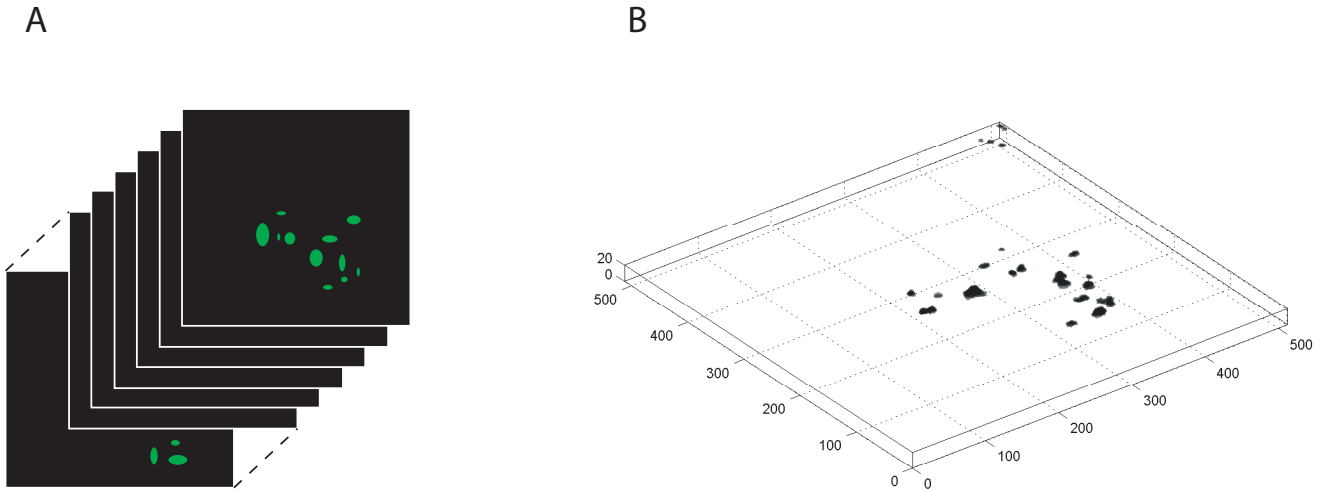


Figure 1. Formation of the 3-D matrix from the confocal image stack of GFP-stained peroxisomes. (A) Schema of the image stack. (B) Binary 3-D matrix after median filtering and thresholding.

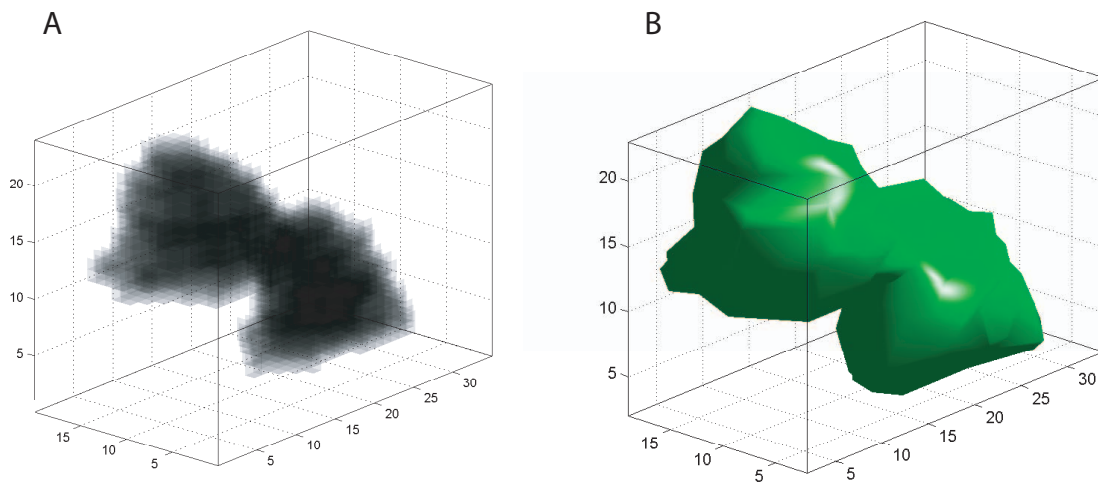


Figure 2. Peroxisomes visualized using two different reconstruction methods. (A) Volumetric reconstruction, where each individual voxel is presented as a semi-transparent cube. (B) Surface reconstruction, where the 3-D shape of the objects surface is approximated and a lighting model applied.

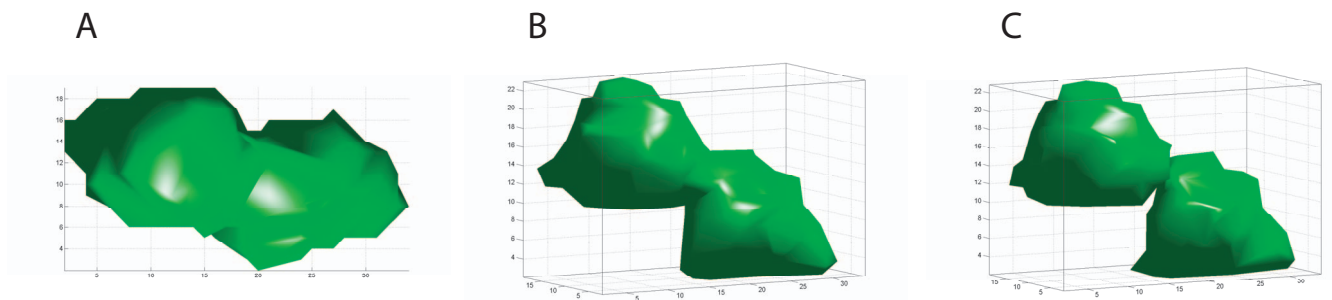


Figure 3. Separation of overlapping peroxisomes. (A) 2-D projection of a peroxisome complex. From this view it is difficult to decide whether there are one or two peroxisomes in the complex. (B) 3-D view of the same complex. (C) Watershed separated peroxisomes. Due to topology of the objects, the gap between the separated peroxisomes can not be clearly visualized.

Table 1. 3-D shape descriptors calculated for two types of objects. The units are in voxels where applicable.

	Volume	Length	Width	Thickness	Compactness	Convexity
Object 1, type 1	2716	32.1	15.7	14.4	182.9	0.8
Object 2, type 2	1336	17.2	14.7	13.4	93.7	1.0
Object 3, type 2	1320	17.7	13.3	13.1	108.0	1.0

selected because, when comparing Figure 3 (B) to (C), they represent objects with clearly different shapes, complexities, and sizes. The descriptor results are given in Table 1. As assumed, volume and length of the complex are significantly larger than of the second and third object, while width and thickness values do not differ significantly. Since compactness is minimized for a simple object (sphere) the first object gives a much larger value than the rest. Convexity, on the other hand, is maximized by an object with a simple shape, so logically the convexity of the first object is the smallest.

4. CONCLUSIONS

We presented methods for straightforward 3-D reconstruction and shape description of peroxisomes from confocal image data. In our case study we showed that with fairly basic image analysis operations having low computational cost, it is possible to enable 3-D shape description with results that correlate well with visual analysis. We also presented how the results from a 3-D image stack often give important additional information about the shapes and peroxisome number, for example, by enabling more precise separation of overlapping objects.

The resolution of confocal microscopy is a limiting factor in detailed analysis. Because we have only a relatively small amount of voxels per peroxisome, just a few falsely segmented voxels can result in significant errors in the shape descriptors. However, the confocal microscope is superior over electron microscopy in enabling high-throughput analysis. In addition to the resolution, the anisotropy and the fact that we discard some of the z -slices also cause inaccuracies in the results. We noticed, however, that the results are consistent over the peroxisomes we imaged, and that neither the visual shapes of the peroxisomes, nor the results of the shape descriptors changed significantly despite the preprocessing steps. To achieve accurate 3-D results, the resolution and contrast of images need to be as high as possible, and therefore the imaging process has to be defined in a consistent and precise manner.

In our future work we will combine the cell segmentation methodology presented in [5] with the peroxisome shape description results presented in this paper. We will also study the effect of deconvolution algorithms to the accuracy of the results. We are implementing all the algorithms into a data analysis pipeline, where acquired images are stored, segmented, and analyzed. This enables automated comparison of shapes of peroxisomes from different cells and different treatments, classification of peroxisomes, and the measurement of the usefulness of the shape descriptors.

5. ACKNOWLEDGMENT

This work was supported by the National Institutes of Health (NIGMS/NIH P50-GM076547) and by the Academy of Finland, (application number 213462, Finnish Programme for Centres of Excellence in Research 2006–2011). AN is supported by the Academy of Finland (application number 120325, Researcher Training and Research Abroad), and RS is supported by Canadian Institutes for Health Research Fellowship.

6. REFERENCES

- [1] R. Cabeza and L. Nyberg, "Imaging cognition II: An empirical review of 275 PET and fMRI studies," *J. Cogn. Neurosci.*, vol. 12, no. 1, pp. 1–47, Jan. 2000.
- [2] B. Hopfenfeld, "A convenient scheme for coupling a finite element curvilinear mesh to a finite element voxel mesh: application to the heart," *Biomed. Eng. Online*, vol. 5, pp. 60, Nov. 2006.
- [3] T. Funkhouser, P. Min, M. Kazhdan, J. Chen, A. Halderman, D. Dobkin, and D. Jacobs, "A search engine for 3D models," *ACM Trans. Graph.*, vol. 22, no. 1, pp. 83–105, Jan. 2003.
- [4] E.J. Garboczi, "Three-dimensional mathematical analysis of particle shape using X-ray tomography and spherical harmonics: Application to aggregates used in concrete," *Cement Concrete Res.*, vol. 32, no. 10, pp. 1621–1638, Oct. 2002.
- [5] A. Niemistö, J. Selinummi, R. Saleem, I. Shmulevich, J. Aitchison, and O. Yli-Harja, "Extraction of the number of peroxisomes in yeast cells by automated image analysis," in *Proc. 28th Ann. Intl. Conf. IEEE Engineering in Medicine and Biology Society (EMBS '06)*, New York, USA, August 30 – September 3, 2006, pp. 2353–2356.
- [6] K. Yamamoto and H.D. Fahimi, "Three-dimensional reconstruction of a peroxisomal reticulum in regenerating rat liver: evidence of interconnections between heterogeneous segments," *J. Cell Biol.*, vol. 105, no. 2, pp. 713–722, Aug. 1987.
- [7] N. Kamasawa, T. Yoshida, M. Ueda, A. Tanaka, and M. Osumi, "Three-dimensional analysis of protein aggregate body in *Saccharomyces cerevisiae* cells," *J. Electron Microsc. (Tokyo)*, vol. 48, no. 2, pp. 173–176, Jan. 1999.
- [8] D.E. Ferrara, D. Weiss, P.H. Carnell, R.P. Vito, D. Vega, X. Gao, S. Nie, and W.R. Taylor, "Quantitative 3D fluorescence technique for the analysis of en face preparations of arterial walls using quantum dot nanocrystals and two-photon excitation laser scanning microscopy," *Am. J. Physiol. Regul. Integr. Comp. Physiol.*, vol. 290, no. 1, pp. R114–R123, Jan. 2006.
- [9] N. Otsu, "A threshold selection method from gray-level histograms," *IEEE. Trans. Systems Man Cybernet.*, vol. 9, no. 1, pp. 62–66, Jan. 1979.
- [10] P. Soille, *Morphological Image Analysis: Principles and Applications*, Springer-Verlag, New York, USA, 2nd edition, 2003.
- [11] B.T. Phong, "Illumination for computer generated pictures," *Commun. ACM*, vol. 18, no. 6, pp. 311–317, Jun. 1975.
- [12] J.C. Russ, *The image processing handbook*, CRC Press LCC, Boca Raton, USA, 1999.
- [13] C. Conrad, H. Erfle, P. Warnat, N. Daigle, T. Lörch, J. Ellenberg, R. Pepperkok, and R. Eils, "Automatic identification of subcellular phenotypes on human cell arrays," *Genome Res.*, vol. 14, no. 6, pp. 1130–1136, Jun. 2004.